

# Quantitative discrimination between endogenous SHG sources in mammalian tissue, based on their polarization response

Sotiris Psilodimitrakopoulos<sup>1</sup>, David Artigas<sup>1,2</sup>, Guadalupe Soria<sup>3</sup>, Ivan Amat-Roldan<sup>1</sup>, Anna M. Planas<sup>3</sup>, and Pablo Loza-Alvarez<sup>1,\*</sup>

<sup>1</sup>ICFO-Institut de Ciències Fotòniques, Mediterranean Technology Park, 08860 Castelldefels (Barcelona), Spain

<sup>2</sup>UPC- Universitat Politècnica de Catalunya, Department of signal theory and communications, 08034, Barcelona, Spain

<sup>3</sup>IIBB-Institut d'Investigacions Biomèdiques de Barcelona, CSIC- Consejo Superior de Investigaciones Científicas, IDIBAPS-Institut d'Investigacions Biomèdiques August Pi-Sunyer, Rossello 161, 08036, Barcelona, Spain

\*pablo.loza@icfo.es

**Abstract:** In this study, the second harmonic generation (SHG) response to polarization and subsequent data analysis is used to discriminate, in the same image, different SHG source architectures with pixel resolution. This is demonstrated in a mammalian tissue containing both skeletal muscle and fibrillar collagen. The SHG intensity variation with the input polarization (PSHG) is fitted pixel by pixel in the image using an algorithm based on a generalized biophysical model. The analysis provides the effective orientation,  $\theta_e$ , of the different SHG active structures (harmonophores) at every pixel. This results in a new image in which collagen and muscle are clearly differentiated. In order to quantify the SHG response, the distribution of  $\theta_e$  for every harmonophore is obtained. We found that for collagen, the distribution was centered at  $\theta_e = 42.7^\circ$  with a full width at half maximum of  $\Delta\theta = 5.9^\circ$  while for muscle  $\theta_e = 65.3^\circ$ , with  $\Delta\theta = 7.7^\circ$ . By comparing these distributions, a quantitative measurement of the discrimination procedure is provided.

©2009 Optical Society of America

**OCIS codes:** (110.5405) Polarimetric imaging; (170.3880) Medical and biological imaging; (170.6935) Tissue characterization; (180.4315) Nonlinear microscopy; (180.5810) Scanning microscopy; (190.2620) Harmonic generation and mixing; (190.1900) Diagnostic applications of nonlinear optics

---

## References and links

1. J. B. Pawley, *Handbook of Biological Confocal Microscopy*, ed. (Springer, Berlin, 2006).
2. W. Denk, J. H. Strickler, and W. W. Webb, "Two-photon laser scanning fluorescence microscopy," *Science* **248**(4951), 73–76 (1990).
3. J. R. Lakowicz, H. Szmajda, K. Nowaczyk, K. W. Berndt, and M. Johnson, "Fluorescence lifetime imaging," *Anal. Biochem.* **202**(2), 316–330 (1992).
4. T. Förster, "Zwischenmolekulare Energiewanderung und Fluoreszenz," *Ann. Phys.* **437**(1-2), 55–75 (1948).
5. J. E. Aubin, "Autofluorescence of viable cultured mammalian cells," *J. Histochem. Cytochem.* **27**(1), 36–43 (1979).
6. Y. R. Shen, "Surface properties probed by second-harmonic and sum-frequency generation," *Nature* **337**(6207), 519–525 (1989).
7. Y. Barad, H. Eisenberg, M. Horowitz, and Y. Silberberg, "Nonlinear scanning laser microscopy by third harmonic generation," *Appl. Phys. Lett.* **70**(8), 922–924 (1997).
8. A. Zumbusch, G. R. Holtom, and X. S. Xie, "Three-dimensional vibrational imaging by coherent anti-stokes raman scattering," *Phys. Rev. Lett.* **82**(20), 4142–4145 (1999).
9. P. J. Campagnola, A. C. Millard, M. Terasaki, P. E. Hoppe, C. J. Malone, and W. A. Mohler, "Three – dimensional high-resolution second harmonic generation imaging of endogenous structural proteins in biological tissues," *Biophys. J.* **82**(1), 493–508 (2002).
10. L. Moreaux, O. Sandre, S. Charpak, M. Blanchard-Desce, and J. Mertz, "Coherent scattering in multi-harmonic light microscopy," *Biophys. J.* **80**(3), 1568–1574 (2001).
11. R. W. Boyd, *Nonlinear Optics*, ed. (Academic, San Diego, CA., 1992).
12. S. Plotnikov, V. Juneja, A. Isaacson, W. Mohler, and P. Campagnola, "Optical Clearing for Improved Contrast in Second Harmonic Generation Imaging of Skeletal Muscle," *Biophys. J.* **90**(1), 328–339 (2006).

#108893 - \$15.00 USD Received 17 Mar 2009; revised 15 May 2009; accepted 20 May 2009; published 2 Jun 2009

(C) 2009 OSA

8 June 2009 / Vol. 17, No. 12 / OPTICS EXPRESS 10168

13. I. Rocha-Mendoza, D. R. Yankelevich, M. Wang, K. M. Reiser, C. W. Frank, A. Knoesen; I. R. Mendoza, "Sum frequency vibrational spectroscopy: the molecular origins of the optical second-order nonlinearity of collagen," *Biophys. J.* **93**(12), 4433–4444 (2007).
14. D. A. Dombeck, K. A. Kasischke, H. D. Vishwasrao, M. Ingelsson, B. T. Hyman, and W. W. Webb, "Uniform polarity microtubule assemblies imaged in native brain tissue by second-harmonic generation microscopy," *Proc. Natl. Acad. Sci. U.S.A.* **100**(12), 7081–7086 (2003).
15. A. C. Kwan, D. A. Dombeck, and W. W. Webb, "Polarized microtubule arrays in apical dendrites and axons," *Proc. Natl. Acad. Sci. U.S.A.* **105**(32), 11370–11375 (2008).
16. S. Psilodimitrakopoulos, I. Amat-Roldan, S. Santos, and M. Mathew, A. Thayil K. N.D. Zalvidea, D. Artigas, P. Loza-Alvarez, "Starch granules as a probe for the polarization at the sample plane of a high resolution multiphoton microscope," *Proc. SPIE* **6860**, 68600E–68600E–11 (2008).
17. S. Roth, and I. Freund, "Second harmonic generation in collagen," *J. Chem. Phys.* **70**(4), 1637–1643 (1979).
18. P. Stoller, K. M. Reiser, P. M. Celliers, and A. M. Rubenchik, "Polarization-modulated second harmonic generation in collagen," *Biophys. J.* **82**(6), 3330–3342 (2002).
19. S. W. Chu, S. Y. Chen, G. W. Chern, T. H. Tsai, Y. C. Chen, B. L. Lin, and C. K. Sun, "Studies of  $\chi^{(2)}/\chi^{(3)}$  tensors in submicron-scaled bio-tissues by polarization harmonics optical microscopy," *Biophys. J.* **86**(6), 3914–3922 (2004).
20. M. Both, M. Vogel, O. Friedrich, F. von Wegner, T. Künsting, R. H. A. Fink, and D. Uttenweiler, "Second harmonic imaging of intrinsic signals in muscle fibers *in situ*," *J. Biomed. Opt.* **9**(5), 882–892 (2004).
21. F. Tiahoo, G. Recher, and D. Rouede, "Estimation of helical angles of myosin and collagen by second harmonic generation imaging microscopy," *Opt. Express* **15**(19), 12286–12295 (2007).
22. C. Odin, T. Guilbert, A. Alkilani, O. P. Boryskina, V. Fleury, and Y. Le Grand, "Collagen and myosin characterization by orientation field second harmonic microscopy," *Opt. Express* **16**(20), 16151–16165 (2008).
23. J. C. Mansfield, C. P. Winlove, J. Moger, and S. J. Matcher, "Collagen fiber arrangement in normal and diseased cartilage studied by polarization sensitive nonlinear microscopy," *J. Biomed. Opt.* **13**(4), 044020 (2008).
24. X. Han, R. M. Burke, M. L. Zettel, P. Tang, and E. B. Brown, "Second harmonic properties of tumor collagen: determining the structural relationship between reactive stroma and healthy stroma," *Opt. Express* **16**(3), 1846–1859 (2008).
25. M. Wang, K. M. Reiser, and A. Knoesen, "Spectral moment invariant analysis of disorder in polarization-modulated second-harmonic-generation images obtained from collagen assemblies," *J. Opt. Soc. Am. A* **24**(11), 3573–3586 (2007).
26. M. Wang, and A. Knoesen, "Rotation- and scale-invariant texture features based on spectral moment invariants," *J. Opt. Soc. Am. A* **24**(9), 2550–2557 (2007).
27. S. Psilodimitrakopoulos, S. I. Santos, I. Amat-Roldan, A. K. Thayil, D. Artigas, and P. Loza-Alvarez, "In vivo, pixel-resolution mapping of thick filaments' orientation in nonfibrillar muscle using polarization-sensitive second harmonic generation microscopy," *J. Biomed. Opt.* **14**(1), 014001 (2009).
28. S. W. Chu, S. P. Tai, C. K. Sun, and C. H. Lin, "Selective imaging in second-harmonic generation microscopy by polarization manipulation," *Appl. Phys. Lett.* **91**(10), 103903 (2007).
29. K. N. Anisha Thayil, E. J. Gualda, S. Psilodimitrakopoulos, I. G. Cormack, I. Amat-Roldán, M. Mathew, D. Artigas, and P. Loza-Alvarez, "Starch-based backwards SHG for in situ MEFISTO pulse characterization in multiphoton microscopy," *J. Microsc.* **230**(Pt 1), 70–75 (2008).
30. K. Beck, and B. Brodsky, "Supercoiled protein motifs: the collagen triple-helix and the  $\alpha$ -helical coiled coil," *J. Struct. Biol.* **122**(1-2), 17–29 (1998).
31. J. Bella, M. Eaton, B. Brodsky, and H. M. Berman, "Crystal and molecular structure of a collagen-like peptide at 1.9 Å resolution," *Science* **266**(5182), 75–81 (1994).
32. S. W. Chu, S. P. Tai, T. M. Liu, C. K. Sun, and C. H. Lin, "Selective imaging in second-harmonic-generation microscopy with anisotropic radiation," *J. Biomed. Opt.* **14**(1), 010504 (2009).

---

## 1. Introduction

High resolution microscopy for biological applications has evolved over the past years driven by the desire to improve 3D image contrast and to distinguish different structural components in a biological sample. Numerous microscopy techniques such as confocal [1], two-photon excited fluorescence (TPEF) [2], fluorescence lifetime imaging (FLIM) [3], or frequency resonant energy transfer (FRET) [4], can be used for these purposes. All these techniques are, however, based on the use of fluorescent markers. For some applications, the incorporation of such fluorophores into the sample is not desirable or acceptable. Thus, high resolution, label free imaging techniques are often used. These are based on light generation through different endogenous mechanisms such as autofluorescence [5], sum frequency generation [6,7], or coherent anti-Stokes Raman scattering (CARS) [8]. In this context, second harmonic generation (SHG) microscopy has lately started to emerge as a technique capable of retrieving in a label free fashion, information on several structural components in tissue [9]. On top of this, SHG microscopy is very attractive for biological imaging as it possesses several interesting properties. Apart from the fact that can be easily implemented in a typical confocal

or two photon laser scanning microscope [10], SHG is a nonlinear scattering phenomenon and, hence, in principle there is no deposition of energy to the interacted matters. Its strength is fully determined by the second-order susceptibility tensor,  $\chi^{(2)}$ , of the nonlinear medium [11]. This tensor is non-vanishing only for non-centrosymmetric media and possesses valuable information on the SHG active architecture at the molecular level. In biological systems, SHG active molecular arrays (harmonophores) can be found in tissue containing muscle [12], collagen [13] and microtubule-based assemblies [9,14,15].

Due to the geometrical characteristics of the local organization of the harmonophores, the detected SHG intensity signal at every point varies when the incoming linear polarization (or the sample) rotates. This technique, referred to as polarization dependent SHG microscopy (or PSHG microscopy) provides a characteristic intensity modulation that has been observed in starch [16], collagen [17,18], and muscle [19,20]. The PSHG analysis has led to the calculation of the mean effective harmonophore orientation angle for myosin or collagen assemblies [12,21,22], and the diagnosis of diseased collagen [23,24]. In addition to this, PSHG combined with signal processing algorithms has also been used for quantitative identification and analysis of structural disorder [25,26]. More recently, by generalizing a biophysical model, we have shown that it is possible to image the orientation of the supporting filaments of the harmonophores in muscle and to quantify their "local" effective orientation and "degree of organization". Importantly, we demonstrated that this can be done without any predefined sample alignment and without the use of any analyzer, greatly simplifying the technique [27]. Finally the problem of discriminating between different SHG active tissue components in the same image has also been addressed (by inserting an analyzer before detecting any SHG signal) [28]. However, there is still the need for characterization and categorization of the different harmonophores as seen in the same image in a quantitative way.

In the present work we provide a methodology, based on PSHG and a generalized biophysical model [27] that allows, in the same image and with pixel resolution, a quantitative discrimination of the different harmonophores present in a sample. Furthermore we show that this is possible without the need of a predefined orientation of the sample and without performing any SHG polarization analysis. The method is demonstrated using rat temporalis muscle in which both skeletal muscle and fibrillar collagen are present.

## 2. Materials and methods

### 2.1 Experimental setup

The experimental setup is based on an adapted inverted microscope (TE2000-U, Nikon, Japan) with the  $y$ - $z$  line scanning unit composed of a pair of galvanometer mirrors (galvos) (Cambridge Technology, UK). A lab-VIEW (National Instruments Corporation) interface program was written to control the raster scanning of the galvos and the data acquisition card. Typical frame acquisition times for a single 500x500 pixel image were 1-2s. A 60x oil-immersion objective [numerical aperture, (NA) = 1.4, Plain Apo-Achromatic, Nikon, Japan] was used throughout the experiments for excitation, while an additional identical objective was used for the collection of the nonlinear signals. For the excitation source, we used a typical Kerr lens modelocked Ti:sapphire laser (MIRA 900f, Coherent, France), with pulses of 160 fs (measured at the sample plane [29]) with a repetition rate of 76 MHz and was operated at a central wavelength of 810 nm.

The average power reaching the sample plane was controlled using a variable neutral density filter wheel. The power was maintained in a range where no observable damage occurred for long imaging periods of time. We placed a linear polarizer after the galvos to reduce any introduced ellipticity. This was followed by a zero order  $\lambda/2$  wave plate (QWPO-810-10-2, CVI Melles Griot), that was placed on a motorized rotational stage (AG-PR100, Newport Corporation) to rotate the linear polarization at the sample plane. Finally, a short-wave-pass dichroic beam splitter (FF720-SDi01-25x36, Semrock Inc) was introduced before the microscope objective. Any effect on the depolarization of the fundamental beam

introduced by the different optical components was assessed, at the sample plane, by measuring the extinction coefficient ratio of the fundamental incident light for every polarization. The measured extinction coefficient ratio, with and without the 60x (NA) = 1.4 objective, was 25:1 and 63:1, respectively.

In the forward direction, a proper mount and detection unit was used. This unit contained the collecting objective, a long-wave-pass dichroic beamsplitter (FF665-Di02-25x36, Semrock Inc), a BG39 filter, a 15-nm FWHM band-pass filter centered at 406 nm (FF01-406/15-25, Semrock Inc) and the photomultiplier tube (PMT) (H9305-04, Hamamatsu, France). The objective lens was mounted on a micrometric 3D translational stage with tilt correction, and the whole unit was enclosed to minimize stray or spurious light into the PMT. The backward propagated signals, after filtered by a BG39 filter and a 15-nm FWHM band-pass filter centered at 406 nm (FF01-406/15-25, Semrock Inc), were collected by a PMT (H9305-04, Hamamatsu, France) placed in one of the output ports of the microscope.

## 2.2 Sample

In the present study experiments were performed in an *ex-vivo* temporalis tissue of adult male Wistar rats. Rats weighted 300–350 g. upon their arrival and were housed in cages with controlled temperature ( $21 \pm 1$  °C) and humidity ( $55 \pm 10\%$ ), with a 12-h light/12-h dark cycle. Rats were sacrificed under deep isofluorane anesthesia by transcardial perfusion with heparinised saline. The left temporalis muscle was dissected and immediately frozen at  $-80$  °C. Coronal sections (30  $\mu$ m thick) were cut on a cryostat (HM 500 Microm, Germany). All sections were on-air mounted between two cover glasses (Marienfeld 24 x 36 mm No. 1, Germany) for subsequent polarization SHG experiments. The temporalis muscle runs along the sides of the cranium, starting in the region of the “temples.” The muscle is involved in the mastication process and it is inserted on the jaw bone. Contraction of the temporalis allows the movement of the jaw while chewing. Collagen is present and serves as the necessary medium to transmit the force generated by the muscle. All experiments were performed in accordance with the National Institutes of Health animal protection guidelines and were approved by the local governmental authorities.

Mammalian skeletal muscle cells are composed of repeated sarcomeric units mainly containing thick and thin filaments of myosin and actin, respectively. The filaments are organized in a specific manner that gives the skeletal muscle a cross-striated appearance. The elements responsible for the SHG signal in muscle are considered to be the thick filaments. These are rigid structures made up of double-helix chiral myosin rods and heads. It has been reported that the SHG source in muscle is contained in the rod domain of myosin’s double helix (two  $\alpha$ -helices) [12]. Furthermore, the spatial arrangement of thick filaments in the transverse direction of a sarcomere follows a hexagonal architecture.

Collagen is an extracellular protein that is the main fibrous component in most organisms. It qualifies as the most widespread structural protein in higher vertebrates and the main means of their structural support. The standard model for the structure of fibrillar collagen is a rising hierarchy of bundled triple helices (collagen molecules) into fibrils. Previous studies have reported that the SHG source in collagen lies in the triple helix of this molecule [12]. As in the thick filaments in muscle, the collagen molecules in the transverse direction have been reported to be arranged in a hexagonal fashion.

## 2.3 The biophysical model and fitting method

Several biophysical models for interpreting the PSHG contrast from collagen and muscle have been proposed in the past [12,19,21,22,27]. The model we use here assumes that the local hexagonal arrangement of SHG source structures in muscle and collagen is translated in a  $C_6$  crystal class system. Then, the nonlinear polarization response  $\vec{P}^{2\omega}$  depends on the incident fundamental electric field, resulting in a radiated SHG electric field. With this geometry, the  $x$  (lab) and the  $x'$  (sample) axis coincides and the relation between the sample and the laboratory frames corresponds to a rotation characterized by an angle  $\varphi$ , giving the orientation of the

main symmetry axis,  $z'$ , of the sample (coincident with the collagen or myosin which are modeled as a collection of rods) with respect to the lab frame. In our experiment the input polarization is rotated clockwise with an angle  $\alpha$  measured with respect to the  $z$ -axis (lab macroscopic frame). Then, assuming that Kleinman's symmetry conditions are valid, the collected intensity in terms of the nonlinear tensor elements is

$$I^{2\omega} \propto I_0 \left\{ \sin^2[2(\phi - \alpha)] + \left[ \sin^2(\phi - \alpha) + \frac{\chi_{33}^{(2)}}{\chi_{15}^{(2)}} \cos^2(\phi - \alpha) \right]^2 \right\}, \quad (1)$$

see [27] for a discussion and detailed description in the deduction of Eq. (1). This Eq. (1) includes information on both the tensor elements ratio and the myosin or collagen rods' orientation.

The model is then expanded to the microscopic (molecular) frame assuming a single axis molecule with dominant hyperpolarizability along this axis, a random distribution in the azimuth angle  $\varphi$ , and a square distribution for the latitude angle  $\theta$ . Then, the effective orientation of the harmonophores can be estimated as [21]:

$$\cos^2 \theta_e = \frac{\chi_{33}^{(2)} / \chi_{15}^{(2)}}{2 + \chi_{33}^{(2)} / \chi_{15}^{(2)}}, \quad (2)$$

where  $\theta_e$  is the PSHG experimentally retrieved effective orientation or helical pitch angle of the SHG source molecule.

Equation (2), gives the key parameter  $\theta_e$  that is used for harmonophore discrimination. Therefore, the objective is to retrieve the ratio  $b = \chi_{33}^{(2)} / \chi_{15}^{(2)}$ . For analysis purpose, Eq. (1) is rewritten as:

$$I^{2\omega} \propto E \left\{ \sin^2 2(\phi - \alpha) + [\sin^2(\phi - \alpha) + b \cos^2(\phi - \alpha)]^2 \right\} + \Delta, \quad (3)$$

where, the free parameters  $E$ ,  $b$ ,  $\varphi$  and  $\Delta$  are retrieved using a fitting algorithm based on a nonlinear least-squares fitting routine (The Mathworks, Champaign-Urbana, IL) using over two thousand iterations per pixel. It has to be noted that Eq. (3) has the extra term  $\Delta$  in comparison to Eq. (1). This is a correction factor that has been added to include experimental errors, the fact that biological sample is not a perfect crystal or any deviation from the theoretical model (mainly, out of plane thick filaments and nonparaxiality of the focused beam) [27]. All these factors introduce a constant background signal (approximately 20% of the total measured intensity).

### 3. Results and discussion

Initially we obtained nine different images of the sample. In each of these, the linear input polarization orientation  $\alpha$  was rotated in steps of  $20^\circ$ . Figure 1(a) corresponds to the superposition of the SHG images for all the polarizations. Here, due to the high magnification used in the experiment, myofibrils can be recognized by the characteristic striation pattern present in muscles. These can be distinguished from other regions forming an almost continuous horizontal line in the Fig. 1(a). These correspond to collagen filaments (note that morphology observation might lead to ambiguities especially when low magnification is used or the sample is damaged). The different images obtained for every polarization were then introduced in the fitting algorithm. Figure 1(b) shows those pixels which were fitted to Eq. (3) with a coefficient of determination  $r^2 > 90\%$ . The coefficient  $r^2$  determines the degree of correlation between the outcome and the values being used for prediction. It varies from 0 to 1 and it provides a measure of how well the model was fitted to the data. Figure 1(b), apart from giving an estimation of the quality of our fitting, is also the result of a filtering mechanism as only those pixels with  $r^2 > 90\%$  were used for the analysis. This helps to remove pixels which are affected by important measurement errors, such as saturation, and those whose dependence on the polarization is not significant, such as fluorescence [23].

The fitting algorithm also retrieved the remaining parameters in Eq. (3): the SHG amplitude  $E$ , the filament orientation  $\phi$  the background parameter  $\Delta$  and the ratio  $b$ . For the purposes of this work, the most interesting information can be obtained from  $b$ , corresponding to the tensor element ratio  $\chi_{33}^{(2)}/\chi_{15}^{(2)}$ . From this parameter and using Eq. (2), the local effective harmonophore orientation  $\theta_e$  can be deduced. Figures 1(c) and 1(d) show (for every

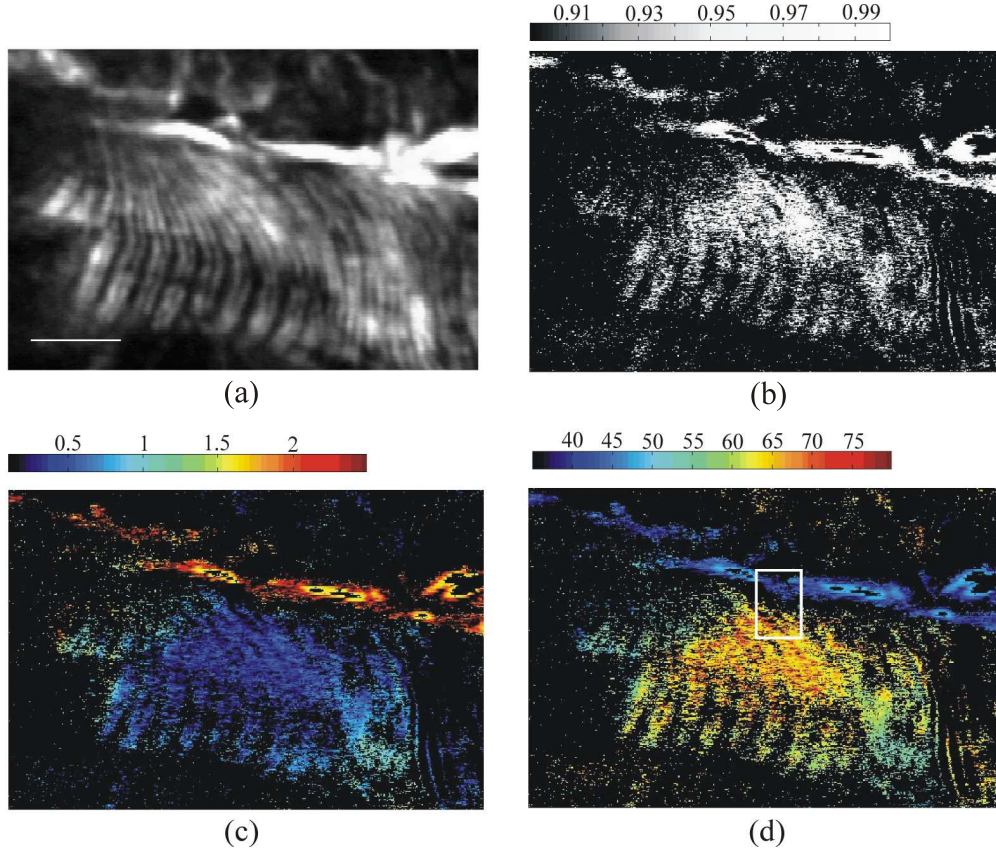


Fig. 1. PSHG at temporalis muscle and analysis. Discriminating between muscle and collagen. (a) Mean SHG intensity of all 9 PSHG images. (b) Image showing the pixels with the coefficient of determination,  $r^2$ , bigger than 90%. (c) Contrast provided by the  $b$  parameter of Eq. (13). (d) Image showing, for every pixel, the effective orientations of harmonophores in degrees. ROI, is shown by the rectangle. Scale bar in panel (a) represents  $10\mu\text{m}$ .

pixel), the ratio  $\chi_{33}^{(2)}/\chi_{15}^{(2)}$  and  $\theta_e$ , respectively. We note that the information contained in those Figs. is similar. In Fig. 1(c) the horizontal line in the upper part of the image results in  $\chi_{33}^{(2)}/\chi_{15}^{(2)} \approx 1.5$  while the central part of the image (composed of vertical lines) corresponds to a  $\chi_{33}^{(2)}/\chi_{15}^{(2)} \approx 0.5$ . This shows that it is possible to distinguish both regions and therefore to differentiate between the two SHG sources. A similar image can be obtained when plotting the amplitude  $E$  (results not shown here). However, the  $\chi_{33}^{(2)}/\chi_{15}^{(2)}$  ratio (or the amplitude  $E$ ) does not identify the SHG source. For that, the local harmonophore orientation,  $\theta_e$ , must be examined. Fig. 1(d) shows that the harmonophore orientation is centred at  $\theta_e \approx 43^\circ$  for the horizontal line and  $\theta_e \approx 65^\circ$  for the vertical lines region. The found harmonophore orientation angles are in agreement to those reported in the literature [12,21,22]. These have been identified to correspond to the helical pitch angle of one collagen's polypeptide chain ( $\sim 45^\circ$ )

and the myosin's  $\alpha$ -helix ( $\sim 68^\circ$ ) [30,31]. Therefore, the angle  $\theta_e$  is the signature identifying and discriminating collagen from muscular tissue in the same image with pixel resolution.

To check this result, we mapped the collagen distribution in our sample by performing a SHG image in the backward direction (as collagen has a larger SHG emission in the backward direction to that compared to muscle [32]). The results are shown in Fig. 2. We can see that the bright horizontal lines appear while those pixels corresponding to muscular tissue show almost no signal. In this way we can qualitatively corroborate that our method has correctly discriminated both tissues.

More information can be extracted from Fig. 1(d) by analyzing the harmonophore distribution in a region of interest (ROI). This is shown in Fig. 3. The effective angular orientation of the harmonophores shows a distribution with two clear, well separated peaks. One is centered at  $\theta_e = 65.3^\circ$  and has a FWHM of  $\Delta\theta = 7.7^\circ$  (muscle) and the second one in which  $\theta_e = 42.7^\circ$  with  $\Delta\theta = 5.9^\circ$  (collagen). In this case, there is no overlap between the two harmonophore angular distributions and therefore, discrimination can be unambiguously performed for every pixel. This methodology allows for a quantification of the discrimination capability between different SHG active sources. In addition, since the measured  $\theta_e$  and  $\Delta\theta$  values are associated to the molecular arrangement (see Eq. (2)), then  $\Delta\theta$  can be associated to the "degree of organization" for the different harmonophores; the smaller the  $\Delta\theta$  is, the more organized the harmonophores structural assemblies are.

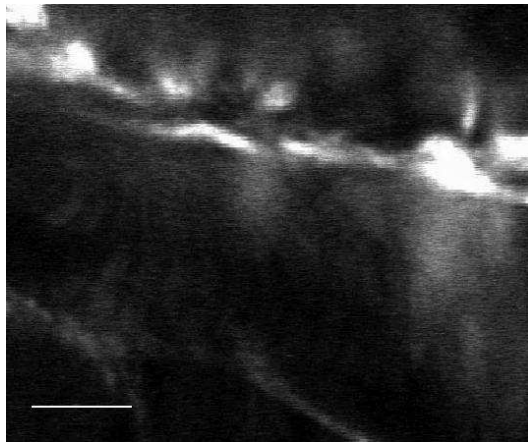


Fig. 2. Backward detected mean SHG intensity of all 9 PSHG images. Scale bar shows  $10\mu\text{m}$

To further explore the capabilities of our method, we proceed to analyze the same sample by changing the number of required images (taken with different input polarizations). As expected when increasing the number of images (more information), then the accuracy of the technique becomes better until reaching a plateau (in our case this was reached with 9 images,

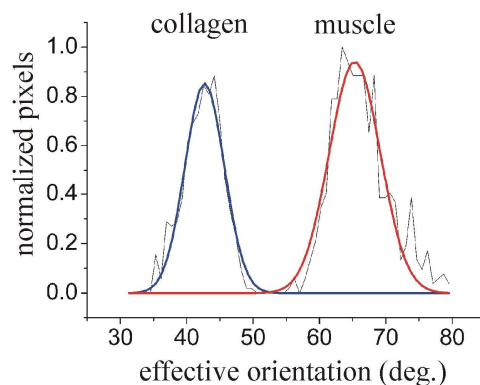


Fig. 3. Histograms and Gaussian fittings calculated for the ROI in Fig. 1(d). For muscle the distribution of the effective orientations of the harmonophores is centered at  $\theta_e = 65.3^\circ$  with a  $\Delta\theta_e = 7.7^\circ$ , while for collagen  $\theta_e = 42.7^\circ$  with a  $\Delta\theta_e = 5.9^\circ$ .

data not shown). Accordingly, it was found that the fewer images used (for the same  $r^2$ ), the broader the distributions are and the less accurate the retrieved means of the distributions are. To demonstrate that here, we run the algorithm with the minimum number of required images (4 images provide the minimum number of equations to fit the 4 parameters of the model). Figure 4 shows the result obtained when polarizations steps of  $\alpha = 0^\circ, 40^\circ, 80^\circ$  and  $120^\circ$  were used. With such small number of images, a fitting with a  $r^2 > 99\%$  (for 5 or more polarizations

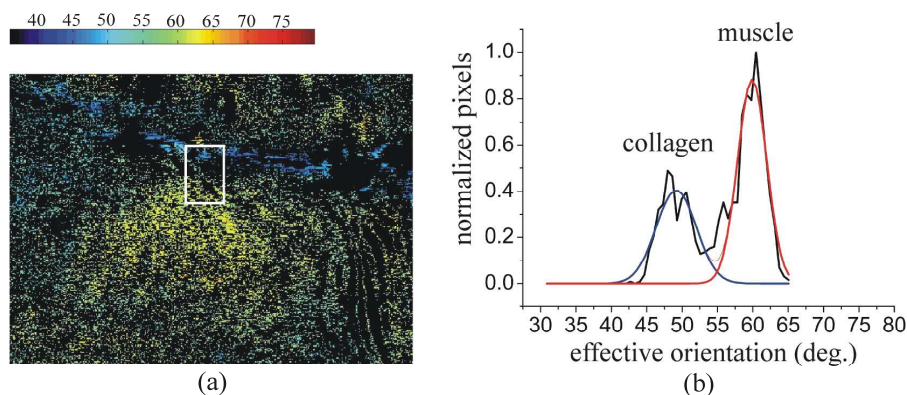


Fig. 4. Fitting using 4 polarization steps:  $\alpha = 0^\circ, 40^\circ, 80^\circ$  and  $120^\circ$  degrees. a) Image showing, for every pixel, the effective orientations of harmonophores (in degrees), after filtering with  $r^2 > 99\%$ . b) Histograms and Gaussian fitting calculated for the ROI in Fig. 4(a). The ROI is placed in the same coordinates as in Fig. 1(d). For muscle the peak of the distribution of the effective orientation of harmonophores is centered at  $\theta_e = 59.9^\circ$  with a  $\Delta\theta_e = 4.1^\circ$ , while for collagen  $\theta_e = 49.2^\circ$  with  $\Delta\theta_e = 5.7^\circ$ .

the  $r^2$  needs to drop in order to retain sufficiently enough pixels inside the ROI) could be found for most of the pixels. Therefore, the  $r^2$  parameter cannot be used to filter the image from those pixels that do not contain the actual information. A direct consequence of this can be seen in Fig. 4(a), where a clear reduction in the contrast (in comparison to Fig. 1(d)) is observed. However, even under this extreme situation it is still possible to visually distinguish in the image among muscle and collagen. This is made more evident in Fig. 4(b) where, as before (see Fig. 3), the harmonophore distribution is calculated (for the same ROI as in Fig. 1(d)). This resulted in a harmonophore orientation angle distribution with peaks at  $\theta_e = 59.9^\circ$  with  $\Delta\theta_e = 4.1^\circ$  (muscle) and  $\theta_e = 49.2^\circ$  with  $\Delta\theta_e = 5.7^\circ$  (collagen). When compared to Fig. 3,

it is found that the distribution shows a shift of the peaks that result in an overlapping region in which the contained pixels cannot be associated to any of the SHG sources. These pixels contain erroneous information that was not filtered using the  $r^2$  parameter. This limits the discrimination capability of the technique. In addition, any other information that can be associated to the measured distribution, such as the “degree of organization”, could also be compromised.

#### **4. Conclusion**

We show that the PSHG imaging technique can be used to discriminate, in a quantitative way, the different SHG active structures present in tissue without any exogenous labelling, any sample alignment or any analysis of the SHG polarization. In particular, this was demonstrated using a mammalian tissue (temporalis muscle) in which two different endogenous SHG active components, myosin and collagen, were present in the same image. This was achieved by measuring the SHG intensity variation on the incoming polarization. The obtained data was fitted into a generalised biophysical model that allowed us to retrieve pixel by pixel, the effective orientation that characterizes the different SHG active structures. This resulted in an image in which the different angular harmonophore orientations,  $\theta_e$ , are mapped. Furthermore, by measuring the frequency distribution of  $\theta_e$ , a pixel-resolution methodology for a quantitative discrimination between harmonophores is presented. In order to explore the limits of the method, we have reduced the required number of polarization images to the theoretical minimum (four). We found that in this case the accuracy of the method was compromised but discrimination was still possible.

#### **Acknowledgements**

This work is supported by the Generalitat de Catalunya and by the Spanish government grant TEC2006-12654 SICO. Authors also acknowledge The Centre for Innovació i Desenvolupament Empresarial-CIDEM (RDITSCON07-1-0006), Grupo Ferrer and the European Regional Development Fund. This research has been partially supported by Fundació Cellex Barcelona.